Density functional study of CO and NO adsorption on Ni-doped MgO(100)

Rosendo Valero,[1,2,a)] José R. B. Gomes,[3,a)] Donald G. Truhlar,[1,a)] and Francesc Illas[4,a)]
[1]*Department of Chemistry and Supercomputing Institute, University of Minnesota, Minneapolis, Minnesota 55455-0431, USA*
[2]*Department of Chemistry, University of Coimbra, Coimbra 3004-535, Portugal*
[3]*CICECO, Department of Chemistry, University of Aveiro, Campus Universitário de Santiago, Aveiro 3810-193, Portugal*
[4]*Departament de Química Física and Institut de Química Teòrica i Computacional (IQTCUB), Universitat de Barcelona, C/Martí i Franquès, Barcelona 08028, Spain*

(Received 22 December 2009; accepted 9 February 2010; published online 9 March 2010)

The adsorption of small molecules such as NO or CO on surfaces of magnetic oxides containing transition metals is difficult to model by current density functional approximations. Two such oxides are NiO(100) and Ni-doped MgO(100). Here we compare the results of a theoretical model of the Ni-doped MgO(100) surface with experimental results on NiO(100), which introduces some uncertainty into a quantitative theory-experiment comparison. In the present work, we tested seven meta-GGA and hybrid metafunctionals, in particular, three developed by the Minnesota group (M05, M06-L, and M06), and TPSS, TPSSh, TPSSKCIS, and B1B95; six GGA functionals, including BP86, PBE, and four other functionals that are modifications of PBE (PBEsol, SOGGA, revPBE, and RPBE); five hybrid GGA functionals (B3LYP, PBE0, B97–2, B97–3, and MPWLYP1M); and one unconventional functional of the generalized gradient type with scaled correlation called MOHLYP. The Minnesota meta-GGA functionals were found in the past to be very good choices when transition metal atoms were present; the other functionals chosen are a selection from the most currently used and most promising sets of functionals for bulk solids and surfaces and for transition metals. The difficulty is due to the charge transfer between open shells in the case of NO and to the weak character of the interaction in the case of CO. It is shown that the M06 hybrid meta functional applied to NO or CO on a model of the Ni-doped MgO(100) surface is able to provide a good description of both adsorbate geometries and binding energies. The M06 vibrational frequency shifts are more accurate than for other functionals, but there is still room for improvement.
 [doi:10.1063/1.3340506]

I. INTRODUCTION

The energy and nature of the chemical bond between an adsorbate and a surface are important factors in electrochemistry, catalysis, corrosion, and electronics.[1,2] Both metal and metal oxide surfaces are important for heterogeneous catalysis. For the interaction of adsorbates with metal surfaces, a reasonable description has been achieved with density functional theory (DFT) applied to periodic slab models.[3–6] However, when the interaction involves metal oxide surfaces, the situation is less clear and obtaining the binding energy of even the simplest neutral molecules such as NH_3, CO, or NO with these surfaces constitutes a complex problem both experimentally and theoretically.[7–19]

Many transition metals form solid solutions with MgO, and such metal-doped MgO materials have varying catalytic capabilities. Ni-doped MgO is particularly interesting and is the subject of this article. Experimentally, the use of a variety of methods for the preparation and cleaning of metal oxide surfaces (epitaxial metal oxide film grown on a metal surface,[20–22] surfaces obtained by cleaving single crystals under ultra high vacuum conditions,[14] metal oxide powder,[7] or sintered polycrystalline metal oxide solid solutions)[11] yields substrates with diverse compositions and different numbers and types of defects; and the adsorbate-substrate bonding energy, especially when weak, is very sensitive to these variables. Nevertheless, the combination of several experimental techniques [infrared (IR) spectroscopy,[11,23–26] thermal desorption spectroscopy,[14,20,21] ultraviolet photoelectron spectroscopy,[21] photoelectron diffraction][22,27,28] and several surface science spectroscopic techniques[29] [such as x-ray photoelectron spectroscopy,[29] or high-resolution electron-energy-loss spectroscopy][29] yielded a clear picture of the geometries and strengths of the interactions of CO, NO, and NH_3 with either the Ni-doped MgO(100) surface or the NiO(100) surface, on which, due in part to a close lattice match of the isostructural MgO and NiO,[20] Ni sites have similar characteristics to Ni sites on Ni-doped MgO.[18,21,25] The number of techniques employed to understand these systems is comparable to previous work aimed to accurately describe adsorption of CO and NO on MgO(001).[2,19,21]

The same investigations traced the influence of surface defects on the adsorbate-surface bonding properties. In the case of CO on NiO(100), which adsorbs in C-down fashion, the ground-state dissociation energy D_0 is 0.30 ± 0.03 eV;[14] and by adding the net loss of zero-point vibrational energy

[a)]Electronic addresses: rvalero@qui.uc.pt, jrgomes@ua.pt, truhlar@umn.edu, and francesc.illas@ub.edu.

upon desorption one obtains an estimated value for the equilibrium dissociation energy, D_e, of 0.37 eV (see Sec. III for more details). The C–Ni and C–O bond lengths are 2.07 ± 0.02 and 1.15 ± 0.09 Å, respectively;[27,28] the Ni–C and C–O bonds are aligned with respect to the surface normal with angles of $\sim 7(+5/-3)°$ and $\sim 12 \pm 12°$, respectively.[27,28] The shift in the C–O stretching frequency upon adsorption is +9 cm^{-1}.[26] Note that this is calculated by subtracting the fundamental vibrational frequency, ω_0, of gas-phase CO, which is 2143 cm^{-1},[30,31] from the experimental C–O stretching vibrational frequency for CO adsorbed on NiO(100), at low coverage, which is 2152 cm^{-1}.[23,26] Similarly, for NO on Ni(100), quantitative structural analysis reveals that the molecule is adsorbed N-down, and the Ni–N bond length is 1.88 ± 0.02 Å with the molecule tilted with respect to the surface normal by $59(+31/-17)°$.[22,27] The experiments also yield $D_0 = 0.57 \pm 0.04$ eV (from which we estimate $D_e = 0.64$ eV) and a vibrational frequency shift in the N–O stretching mode of −75 cm^{-1} (1801 cm^{-1} IR peak observed at low coverage,[23] shifted with respect to the experimental[32] fundamental frequency of NO, 1876 cm^{-1}).

When an embedded cluster model is used to model adsorption of CO, NO, and other adsorbates on oxide surfaces, one needs to consider the cluster size, the type of embedding scheme, and the basis set used to describe the electron density, and one also has to select an adequate and computationally affordable electronic structure method. For the latter, DFT is a common choice, although many popular density functionals (i.e., exchange-correlation functionals) do not accurately describe weak interactions between adsorbates and surfaces. On the other hand, wave function theory (WFT) methods in the form of configuration interaction (CI), many body perturbation theory, or coupled cluster theory are restricted by their cost to relatively small model systems, and CI is not size extensive. The successes and failures of current theoretical methods for the description of the interaction between CO and the regular sites of MgO(100) were summarized recently,[19] and it was also shown that recent hybrid metafunctionals from the M06 family[33] perform well both for the calculation of the interaction energy and for the prediction of the positive and small stretching vibrational frequency shift of CO. The good behavior of the M06 family of functionals for the bonding of CO to MgO(100) prompted us to perform the present study on the interaction of CO and NO with the Ni-doped MgO(100) surface.

The difficulties of using DFT to describe the interaction of NO with NiO(100) or with Ni-doped MgO(100) have been described in detail by Di Valentin *et al.*,[15] and in most aspects the difficulties are similar to those for CO.[15,18] However, NO provides the possibility of gathering information about the spin distribution through electron paramagnetic resonance measurements.[34] For the particular case of the interaction between NO and Ni-doped MgO(100) it has been found that the bonding has not been well described by the density functional approximations applied so far, and spin-polarized DFT can give reasonable adsorption properties only at the cost of a wrong spin distribution. Moreover, various exchange-correlation functionals give different answers that vary from strongly bound to strongly unbound, with the origin of this difference being attributable to different descriptions of the Coulomb repulsion within the 3d subshell. Therefore the accurate inclusion of dynamical correlation is essential. The bonding is dominated by long-range electrostatic and inductive forces and is also strongly affected by the Pauli repulsion, especially, in the case of CO adsorption, between the 5σ orbital of CO and the almost fully occupied 3d subshell of Ni^{2+}.[35] Furthermore, most DFT functionals are challenged to provide an accurate treatment of the dispersionlike contributions to the interaction energy. Note that the interaction of CO with the Ni-doped MgO(100) surface does not lead to any spin redistribution—CO remains closed shell, and Ni^{2+} remains a local triplet—whereas the interaction of NO with the same surface involves a significant spin redistribution—the unpaired NO electron is transferred to Ni^{2+} which is reduced to Ni^{+} and becomes locally a doublet with a d^9 electronic configuration.[18] Thus it appears that the simultaneously correct description of the interactions of NO and CO with NiO(100) and with Ni-doped MgO by a single exchange-correlation functional will be challenging.

The difficulties encountered in properly describing the interactions of CO or NO with Ni-doped MgO(100) or NiO(100) surfaces triggered a considerable amount of theoretical research work.[18,21,29,35–42] A selection of the most relevant results is presented in Tables I and II for NO and CO, respectively. In the works published so far, a variety of theoretical approaches and surface models have been used, with some calculations including a counterpoise correction (CpC) for basis set superposition error (BSSE) and other calculations omitting this. Most studies include the adsorbate binding energy and equilibrium geometry, and a subset of the studies also considered the N–O or C–O vibrational frequency shifts.

All DFT calculations involve a Kohn–Sham determinant corresponding to a model system of noninteracting electrons with the same density as the system of interest; the doubly occupied spin orbitals of this determinant may be restricted to have identical spatial orbitals, or they may be unrestricted. All DFT calculations in this article are unrestricted (sometimes called spin polarized) except for four cases in Table I where a prefix RO is used to denote restricted open-shell.

Table I shows that several of the tested methodologies, both DFT and WFT, have severe problems in accurately describing the NO-surface interaction. Embedded cluster model calculations using a variety of BSSE-corrected WFT and DFT methods (ROHF, ROHFLYP,[15] ROB3LYP,[43–46] ROMPW1PW91,[47] and CASSCF) predict repulsive interactions, while other methods (CI, B3LYP, and ROCASPT2) yield BSSE-corrected binding energies that are systematically lower than the experimental result (an equilibrium dissociation energy D_e of 0.64 eV obtained by adding the estimated zero point vibrational energy to the experimental[14] zero-point dissociation energy D_0). Furthermore, all theoretical approaches tested so far give equilibrium N–O distances larger than the 1.12 ± 0.05 Å best-fit-experimental bond length for adsorbed NO.[22] Nevertheless, the calculated Ni–N–O angles are in excellent agreement with the reported experimental value, $59(+31/-17)°$,[22] with a single exception, i.e., the work due to Kuhlenbeck *et al.*,[29] where a model with

TABLE I. Comparison of computational and experimental results from the literature for NO adsorption on Ni-doped MgO(100) or NiO(100) surfaces (for angles definition see Fig. 2).

Method	Reference	Basis set	Model	Coverage (ML)	D_e without CpC (eV)	D_e with CpC (eV)	R(Ni–N) (Å)	R(N–O) (Å)	θ(Ni–N–O) (deg)	$\Delta\omega_e$ (cm^{-1})
CI	29	TZP	NiO_5^{8-}+PC			0.17	2.1 (fixed)		50	
ROHF	15	TZP(Ni,N,O)/DZ(Mg)	$NiMg_8O_9$+TIP+PC			−4.29	1.85	1.153	64	
ROHFLYP	15 and 18	TZP(Ni,N,O)/DZ(Mg)	$NiMg_8O_9$+TIP+PC		−3.42	−3.53	1.82	1.148	64	−404
ROB3LYP	15 and 18	TZP(Ni,N,O)/DZ(Mg)	$NiMg_8O_9$+TIP+PC		0.00	−0.11	1.85	1.164	61	−209
B3LYP	18	TZP(Ni,N,O)/DZ(Mg)	$NiMg_8O_9$+TIP+PC		0.36	0.25	2.02	1.153	57	−110
ROBLYP	15 and 18	TZP(Ni,N,O)/DZ(Mg)	$NiMg_8O_9$+TIP+PC		1.10	0.96	1.84	1.191	60	−292
ROMPW1PW91	15	TZP(Ni,N,O)/DZ(Mg)	$NiMg_8O_9$+TIP+PC			−0.20	1.83	1.158	62	
ROCASPT2	15 and 18	TZP(Ni,N,O)/DZ(Mg)	$NiMg_8O_9$+TIP+PC		0.65	0.48	2.03	1.173	63	−101
CASPT2	39	TZP(Ni,N,O)/DZ(Mg)	$NiO_5Mg_{13}^{18+}$+PC		0.70	0.34	1.99	1.17	58	
CASPT2	39	ANO	$NiO_5Mg_{13}^{18+}$+PC		0.53	0.38	1.99[a]	1.17[a]	58[a]	
CASPT2	39	TZP(Ni,N,O)/DZ(Mg)	$Ni_3O_{11}Mg_{23}^{30+}$+PC		0.79	0.41	1.99[a]	1.17[a]	58[a]	
CASSCF(3,3)	39	TZP(Ni,N,O)/DZ(Mg)	$NiO_5Mg_{13}^{18+}$+PC		−0.37	−0.46	1.9[a]	1.17[a]	58[a]	
PW91	21	PW/USPP	$Ni_{0.06}Mg_{0.94}O(100)$ Four-layer slab	0.25	0.74		1.85	1.19		
LSDA	40	PAW/330 eV	NiO(100) slab	0.5	1.32		1.72	1.175	54	
PW91	40	PAW/330 eV	NiO(100) slab	0.5	1.24		1.76	1.185	52	
LSDA+U	40	PAW/330 eV	NiO(100) slab	0.5	0.67		1.78	1.168	56	
PW91+U	40	PAW/330 eV	NiO(100) slab	0.5	0.40		1.98	1.174	55	
Experimental					0.64[b]	0.64[b]	1.88 ± 0.02 [c]	1.12 ± 0.15 [d]	59 ± 24 [d]	−75[e]

[a]CASPT2/TZP geometry.
[b]Calculated from the experimental (Ref. 14) D_0 value of 0.57 ± 0.04 eV value together with the soft modes of frequencies 17, 34, 149, 169, and 225 cm^{-1} obtained with the M06 functional for the $NO-NiMg_8O_9$ cluster, and taking into account the decrease $\Delta\omega_e$ in the NO mode.
[c]References 22 and 27.
[d]Reference 22.
[e]Reference 23.

a frozen Ni–N distance was used. The calculated Ni–N bond lengths are within 0.15 Å of the experimental result,[22,27] 1.88 ± 0.02 Å. The calculated vibrational frequency shifts (ROHFLYP, ROB3LYP, B3LYP, ROBLYP,[43,44] and ROCASPT2) are more negative than the experimentally derived shift (−75 cm^{-1}); the B3LYP and ROCASPT2 are 39 and 30 cm^{-1} more negative than the experimental result while the other three computational approaches give larger deviations from experiment (differences of 138–333 cm^{-1}). Interestingly, the methods that give better predictions of the vibrational frequency shift (B3LYP and ROCASPT2) are those that yield the largest adsorbate-to-surface distances, i.e., largest Ni–N lengths. Globally, the ROCASPT2 approach together with the embedded $NiMg_8O_9$ cluster model gives the best results of the WFT methods, in particular the best interaction energy and vibrational frequency shift, but it still yields a quite too long adsorbate-to-surface distance.

Periodic DFT approaches using LSDA and GGA-type exchange-correlations functionals, commonly used in surface science and condensed matter applications, have also been applied to the NiO surface. LSDA and GGA methods predict that NO binds to the surface, but the addition of a Hubbard-type on-site Coulomb repulsion term (U) to spin-polarized (i.e., unrestricted) LSDA and PW91 (which is a GGA) significantly improves both the calculated interaction energies and also the optimized geometrical parameters.[40] The PW91+U method gave better agreement.[40] However, Rodriguez *et al.*[21] and Rohrbach and Hafner[40] do not provide vibrational frequencies for the NO-oxide systems, and therefore it is not possible to test their models for the N–O vibrational frequency shifts.

In the case of CO on the NiO(100) and Ni-doped MgO(100) oxide surfaces (cf. Table II), the picture is very similar to that described above for NO. The calculated interaction energies are again significantly affected by BSSE when cluster models are used, and the calculated interaction energies are systematically lower than the experimental[14] result (D_e=0.37 eV, obtained by adding the estimated zero point vibrational energy to the experimental D_0 $=0.30 \pm 0.03$ eV). The large number of theoretical approaches and models that have been used allow one to extract valuable information from Table II. Increasing the number of explicit O and Mg ions around the central Ni cation and keeping the model frozen (entries 2 and 3 in Table II) has a negligible effect on the BSSE-corrected interaction energy, but increasing the number of Ni cations in the model (entries 3 and 4) almost doubles the calculated interaction energy. Using the ANO basis set instead of the TZP one, also on a frozen model, increases the calculated interaction energy by 30% (entries 2 and 5). Furthermore, both RCCSD or RCCSD(T) give less positive binding energies when compared with MP2 (entries 2, 7, and 8). The introduction of electron correlation by DFT improves the description of the CO/oxide interaction (entries 10–15). As for NO, the BLYP approach yields the largest binding energy, but in the case of CO the value is closest to the experimental result rather than overshooting it. Importantly, the use of models mimicking the Ni(100) surface or the Ni-doped MgO(100) surface noticeably affects the calculated energies (entries 12–15). Finally, the ROCASPT2 calculated vibrational frequency shift is in very good agreement with the experimental result (+9 cm^{-1}, Ref. 26) and the UHF and HFLYP values are also

TABLE II. Comparison of computational and experimental results from the literature for CO adsorption on Ni-doped MgO(100) or NiO(100) surfaces (for angles definition see Fig. 2).

Method	Reference	Basis set	Model	Coverage (ML)	D_e without CpC (eV)	D_e with CpC (eV)	R(Ni–C) (Å)	R(C–O) (Å)	θ(Ni–C–O) (deg)	$\Delta\omega_e$ (cm^{-1})
HF	35	TZP	$Ni(H_2O)_3(OH)_2$		0.51	0.08	2.86	1.11 (fixed)		
RMP2	39	TZP(Ni,N,O)/DZ(Mg)	$NiO_5Mg_{13}^{18+}$+PC		0.40	0.10	2.15	1.14		
RMP2	39	TZP(Ni,N,O)/DZ(Mg)	$NiO_{17}Mg_{37}^{42+}$+PC		0.52	0.11	2.15[a]	1.14[a]		
RMP2	39	TZP(Ni,N,O)/DZ(Mg)	$Ni_5O_{17}Mg_{33}^{42+}$+PC		0.54	0.20	2.15[a]	1.14[a]		
RMP2	39	ANO	$NiO_5Mg_{13}^{18+}$+PC		0.28	0.13	2.15[a]	1.14[a]		
ROHF	39	TZP(Ni,N,O)/DZ(Mg)	$NiO_5Mg_{13}^{18+}$+PC		−0.21	−0.29	2.15[a]	1.14[a]		
RCCSD	39	TZP(Ni,N,O)/DZ(Mg)	$NiO_5Mg_{13}^{18+}$+PC		0.33	0.02	2.15[a]	1.14[a]		
RCCSD(T)	39	TZP(Ni,N,O)/DZ(Mg)	$NiO_5Mg_{13}^{18+}$+PC		0.43	0.09	2.15[a]	1.14[a]		
CASSCF(18,13)	39	TZP(Ni,N,O)/DZ(Mg)	$NiO_5Mg_{13}^{18+}$+PC			−0.30	2.15[a]	1.14[a]		
UHF	41	6-311+G(d,p) (CO) 8-6411G41d (Ni) 8-411G1d (O, cluster)	Ni_9O_9+TIP+PC		0.15	0.00	2.92	1.105		0
HFLYP	41	TZP	Ni_9O_9+TIP+PC		0.22	0.15	2.38	1.098		−10
B3LYP	41	TZP	Ni_9O_9+TIP+PC		0.12	0.02	2.10	1.134		−73
B3LYP	18	TZP(Ni,N,O)/DZ(Mg)	$NiMg_8O_9$+TIP+PC		0.16	0.06	2.10	1.130		
BLYP	41	TZP	Ni_9O_9+TIP+PC		0.33	0.23	1.87	1.161		−172
BLYP	18	TZP(Ni,N,O)/DZ(Mg)	$NiMg_8O_9$+TIP+PC		0.41	0.30	1.90	1.154		
ROCASPT2	18	TZP(Ni,N,O)/DZ(Mg)	$NiMg_8O_9$+TIP+PC NiO(100)		0.30	0.13	2.24	1.136		+16
HFLYP	41	6-311+G(d,p) (CO) 8-6411G41d (Ni) 8-411G1d (O, cluster)	three-layer slab	0.25	0.29	0.17	2.40	1.095		−3
PW91	21	PW/USPP	$Ni_{0.06}Mg_{0.94}O(100)$ Four-layer slab	0.25	0.61		1.93	1.14		
LSDA	42	PAW/330 eV	NiO(100) slab	0.5	1.26		1.76	1.150	0	
PW91	42	PAW/330 eV	NiO(100) slab	0.5	0.70		1.81	1.153	0	
LSDA+U	42	PAW/330 eV	NiO(100) slab	0.25	0.80		1.93	1.144	11	
LSDA+U	42	PAW/330 eV	NiO(100) slab	0.5	0.79		1.94	1.145	18	
PW91+U	42	PAW/330 eV	NiO(100) slab	0.25	0.33		2.03	1.143	15	
PW91+U	42	PAW/330 eV	NiO(100) slab	0.5	0.26		2.04	1.145	21	
Experimental						0.37[b]	2.07 ± 0.02[c]	1.15 ± 0.09[c,d]	12 ± 12[c,d]	+9[e]

[a]RMP2/TZP geometry.
[b]Calculated from the experimental (Ref. 14) D_0 value of 0.30 ± 0.03 eV for D_0 with the soft modes of frequencies 128, 170, 216, 318, and 318 cm^{-1} obtained with the M06 functional for the CO–$NiMg_8O_9$ cluster, and taking into account the decrease $\Delta\omega_e$ in the CO mode.
[c]Reference 27.
[d]Reference 28.
[e]Reference 26.

close; the BLYP calculated value is too low, and the B3LYP approach, which includes 20% HF exchange, is between the calculated BLYP (no HF exchange) and the UHF (100% HF exchange) shifts. The results obtained with periodic slab models follow the same pattern as those already described for NO; in particular, the inclusion of Hubbard-type on-site Coulomb repulsion in the calculations significantly improves the calculated interaction energies.[40]

The most important conclusions drawn from Tables I and II are (i) most of the approaches used in previous works underestimate the substrate-adsorbate bonding energy for both NO and CO and (ii) they also fail to describe the structure of the adsorbed molecule. The latter has negative implications for the accuracy of the calculated vibrational frequency shifts. The good performance of the M06 hybrid metafunctionals in describing several difficult systems[19,48] prompted us to test their performance, and also that of the M05 family, in describing the interaction of CO and NO with the Ni-doped MgO(100) surface described by appropriate embedded cluster models. Several other functionals that have been proposed for solid-state and surface science studies and for transition metals are also included in the study.

II. COMPUTATIONAL DETAILS

The interaction of CO and NO with an isolated Ni^{2+} impurity on the MgO(100) surface was modeled with two different stoichiometric cluster models that are shown in Fig. 1. In the two models, a central Ni atom is surrounded by 8 Mg and 9 O atoms or by 24 Mg and 25 O atoms, keeping (initially) an undistorted MgO rock-salt structure and with all electrons treated explicitly. (As discussed later in this section, the coordinates of six or more of the atoms are relaxed in the presence of adsorbate in a subsequent optimization step.) The resulting $NiMg_8O_9$ and $NiMg_{24}O_{25}$ cluster models were embedded in an environment that accounts for short- and long-range interactions with the remainder of the crystal,[49–56] and, in particular, that accounts for the long-

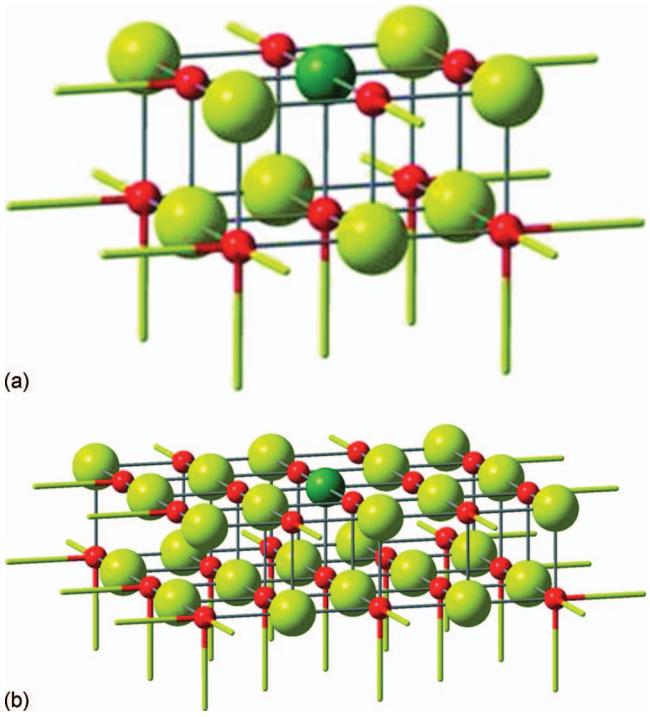

FIG. 1. (a) $NiMg_8O_9$ and (b) $NiMg_{24}O_{25}$ cluster models (ball and stick) and TIPs (sticks) used to simulate the Ni-doped MgO(100) surface. Large yellow balls, small red balls, and green medium balls denote Mg^{2+}, O^{2-}, and Ni^{2+} ions, respectively. The array of PCs is not shown.

range Madelung potential. The embedding scheme considered both total ion potentials (TIPs) and a large array of point charges (PCs). Each TIP is a pseudopotential simulating a Mg^{2+} cation directly coordinated to the oxygen anions at the cluster edge. The cluster plus TIPs were further surrounded by PCs with values of $\pm 2e$. In particular, the $NiMg_8O_9$ cluster is surrounded by 17 TIPs, 312 positive PCs, and 329 negative PCs, and for the $NiMg_{24}O_{25}$ cluster these numbers are 33, 280, and 313, respectively. These two cluster models are identical to those used in a very recent study concerning the adsorption of CO on the MgO(100) surface but with the central Mg atom substituted by a Ni atom,[19] and they are large enough to provide meaningful results although obtaining converged results may require expanding the quantum region further. Nevertheless, there is evidence that enlarging the cluster model will at most increase adsorption energies by 0.15 eV (Ref. 39) and hence will not change the main conclusions of the present work.

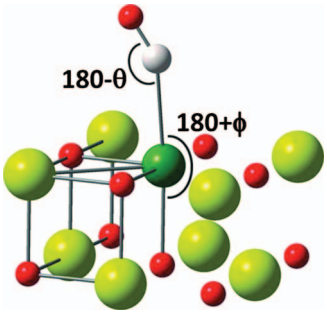

FIG. 2. Definition of the angles θ and ϕ. Large yellow balls, small red balls, and green medium balls denote Mg^{2+}, O^{2-}, and Ni^{2+} ions, respectively.

A combination of basis sets has been used. The Ni atom was described by the new contracted LANL2TZ+ basis set,[57] which was derived from the older LANL2DZ basis set,[58] and that has been proposed to be more suitable for DFT calculations.[57] The five O atoms linked directly to the Ni atom were represented by the standard 6-31+G(d) basis set. The other surface O atoms as well as the Mg atoms were described with the 6-31G basis. The Ahlrichs' TZVP basis set[59] was used for the CO and NO molecules.

The density functionals considered here contain various elements. An LSDA depends only on spin densities (that is, the densities of up-spin and down-spin electrons), and a GGA also depends on the gradients of the spin densities. A meta-GGA adds spin kinetic energy to a GGA, a hybrid GGA adds Hartree–Fock (HF) exchange to a GGA, and a hybrid metafunctional adds both. Functionals without HF exchange are sometimes called local.

In our choice of density functionals we have been guided by previous studies of the performance of the functionals of the M0*x* family for a large number of systems and properties.[33,60–62] From these studies it was concluded that only functionals with less than 30% HF exchange should be used for systems involving transition metal atoms. Thus, the M06-L (Ref. 60) and M06 (Ref. 61) functionals of the M06 family and the M05 (Ref. 62) functional from the M05 family were employed in the calculations. These functionals incorporate kinetic-energy density in a balanced way in the exchange and correlation functionals. The three functionals differ essentially in the inclusion or absence of a percentage of HF exchange, in the functional forms used to represent exchange and correlation, and in parametrization. The percentages of HF exchange in the functionals are 0%, 27%, and 28% for M06-L, M06, and M05, respectively.[33,60–62] M06-L is a meta-GGA, and M05 and M06 are hybrid metafunctionals.

We also tested several functionals that are frequently used in solid-state and surface science studies, including six GGA functionals, namely, BP86,[43,63] Perdew–Burke–Ernzerhof (PBE),[64] and four modifications of PBE, namely, PBEsol,[65] SOGGA,[66] revised PBE (revPBE),[67] and RPBE;[6] five hybrid GGA functionals, including the popular B3LYP functional, the MPWLYP1M functional with one parameter adjusted for metals,[68] PBE0[69,70] (the hybrid version of PBE with 25% HF exchange), B97-2,[71] and B97-3;[72] and four additional meta-GGA and hybrid metafunctionals, namely, the meta-GGA of Tao, Perdew, Staroverov, and Scuseria (TPSS);[73] its hybrid meta version with 10% of HF exchange, called TPSSh;[74] the TPSSKCIS combination meta-GGA;[68,75–77] and the B1B95 hybrid metafunctional.[43,78] Finally, the unconventional functional of the generalized gradient with scaled correlation type, MOHLYP,[68] was also included.

The BP86 functional is a combination of Becke's 1988 (Ref. 43) exchange functional and Perdew's 1986 (Ref. 63) correlation functional, and was used to study the adsorption of CO on MgO(100) (see references cited in Ref. 19) with moderate success. The Perdew–Burke–Ernzerhof (PBE) (Ref. 64) functional was constructed to satisfy several energetically relevant physical constraints and is, along with the

Perdew–Wang 91 (PW91)[79–81] functional, one of the most widely employed functionals in condensed-matter studies. The PBEsol (Ref. 65) functional modifies PBE by optimizing one parameter to fit the jellium-surface exchange correlation. Lattice constants were found to be more accurate with PBEsol than with PBE, and by construction PBEsol gives improved jellium surface energies. Thus, it was hoped by its developers that it would provide good results for interactions on real surfaces. The SOGGA (Ref. 66) (second-order GGA) functional recently developed in the Minnesota group introduces a modification of the PBE exchange functional that restores the density-gradient expansion for both exchange and correlation to second order and enforces a tighter Lieb–Oxford bound than other GGAs. The correlation functional is the same as the PBE one. SOGGA functional has been shown to improve lattice constants by 20% compared to PBEsol. The revPBE (Ref. 67) functional is identical to PBE but for a one-parameter modification in the exchange part of PBE based on a fit to exchange-only total atomic energies. The atomization energies given by revPBE were shown to improve the PBE ones for a large database of small molecules. The RPBE (Ref. 6) functional is a slight revision of PBE with a new functional form for the exchange enhancement factor that, unlike revPBE, fulfills the local Lieb–Oxford bound. The chemisorption energies of atoms and molecules on transition-metal surfaces obtained with revPBE and RPBE are normally very similar[6] and represent in many cases a significant improvement over PBE. However, RPBE does not improve on PBE for jellium surface energies, lattice constants, and bulk moduli of solids[82] and bond distances of main-group compounds.[66] As RPBE has been used in a plethora of theoretical studies of solids and gas-surface systems (see for instance Refs. 5 and 83), it is very interesting to assess its accuracy for the adsorption of CO and NO on a Ni-doped MgO(100) surface.

The popular B3LYP[43–46] hybrid GGA functional has been the density functional most widely used by chemists for many years, and it still represents about 80% of the total occurrences of density functionals in the chemical literature.[84] However, in applications to surface science studies, B3LYP is rarely the best-performing functional. The MPWLYP1M (Ref. 68) hybrid GGA functional is a combination of 95% MPW exchange plus 5% HF exchange and of LYP correlation, with one parameter optimized for metals. This functional was optimized against a data set of metal-ligand and metal-metal bond energies (with both main-group and transition metals), main-group atomization energies, atomic ionization potentials, and bond lengths. The PBE0[69,70] hybrid derives from PBE and contains 25% HF exchange. PBE0 has been shown to be a better compromise than PBE for both molecular atomization energies and solid-state properties. The functional form of the B97-2 (Ref. 71) and B97-3 (Ref. 72) functionals is a generalization of that of Becke's 1997 (B97) (Ref. 85) exchange-correlation functional, adding more parameters that are fitted to experimental data (mainly thermochemical quantities and reaction barriers).

As mentioned above, in addition to the M06-L meta-GGA functional and the M05 and M06 hybrid metafunctionals of the M0*x* family, two other metafunctionals and two other hybrid metafunctionals were included in the present study. TPSS (Ref. 73) is a meta-GGA designed in an attempt to give a balanced overall description of both molecules and solids.[74,86] Furthermore, TPSS has been shown to be, along with PBEsol, one of the best functionals for jellium surface energies.[65,74] The hybrid version of TPSS with 10% HF exchange, TPSSh,[74] represents an improvement to TPSS for some thermochemical properties, bond lengths, and frequencies of the molecules in the G3/99 test set. The TPSSKCIS[68,75–77] functional is a combination of TPSS exchange with the KCIS correlation functional and was found to be one of the best functionals for a database of energies of main-group and transition metal compounds.[68] The B1B95[43,78] functional is a one-parameter hybrid meta-GGA that combines Becke's 1988 exchange[43] and 1995 kinetic-energy-dependent correlation,[78] and it was shown in one study[87] to be among the best general-purpose hybrid functionals tested for thermochemical kinetics.

Another functional tested in the present work is the MOHLYP (Ref. 68) functional. In MOHLYP, "HLYP" stands for 50% LYP correlation (i.e., "half-LYP") and "MO" means a metal-optimized OptX functional. This functional was optimized against a database of energies and bond lengths containing transition metals.

An important question we wanted to address in the present study and which partly motivated our choice of density functionals is whether, and to what extent, a good description of jellium surface energies implies good gas-surface adsorption energies. A detailed discussion of this point is presented below.

For all the density functionals employed and for the two cluster models considered [$CO(NO)/NiMg_8O_9$ and $CO(NO)/NiMg_{24}O_{25}$], the coordinates of the central Ni atom, of the five O atoms surrounding Ni, and of the adsorbates (NO or CO) have been fully optimized, with the rest of the atoms and TIPs kept frozen at the bulk geometry. Geometries were optimized without a CpC (Ref. 88) for BSSE, and then the CpC was applied at this geometry. Vibrational frequencies were calculated with the PCs fixed but with all atoms and TIPs allowed to relax. Thus, the dimension of the block of the Hessian matrix considered is 111×111 for $CO(NO)/NiMg_8O_9$. The frequencies for the large cluster, $CO(NO)/NiMg_{24}O_{25}$, were not calculated due to computational limitations. No corrections for anharmonicity were considered for the theoretical frequencies. All the calculations were performed with a locally modified version of GAUSSIAN03 Revision D.01,[89] employing the MN-GFM module.[90]

III. RESULTS and DISCUSSION

The calculated results for the NO species interacting with each of the cluster models considered in the present work are reported in Tables III and VI, where Table III has the results for the larger model (frequency and shifts calculated with the small model) and Table VI shows the results

TABLE III. Calculated results for gas-phase NO (values in parentheses) and for N-down adsorbed NO at a Ni^{2+} site on the Ni-doped MgO(100) surface. (For angles definition see Fig. 2; $NiMg_{24}O_9$ model for $\langle \hat{S}^2 \rangle$, D_e, R, and θ; $NiMg_8O_9$ model for ω_e and $\Delta\omega_e$. Values in parentheses are for separated NO.)

Method	$\langle \hat{S}^2 \rangle$	D_e (eV)	R(Ni–N) (Å)	R(N–O) (Å)	ϕ(O–Ni–N) (deg)	θ(Ni–N–O) (deg)	ω_e (cm^{-1})	$\Delta\omega_e$ (cm^{-1})
B3LYP	1.55	0.27, 0.15[a]	2.09	1.149 (1.147)	3	57	1887 (1974)	−87
M06-L	1.18	0.92, 0.79	1.89	1.165 (1.150)	3	59	1772 (1970)	−198
M06	1.49	0.58, 0.46	2.03	1.143 (1.141)	3	58	1928 (2029)	−101
M05	1.48	0.38, 0.25	2.03	1.144 (1.144)	4	58	1936 (2030)	−94
SOGGA	0.87	1.55, 1.38	1.79	1.175 (1.156)	3	60	1699 (1924)	−225
PBE	0.94	1.10, 0.94	1.83	1.178 (1.160)	3	59	1679 (1889)	−210
PBEsol	0.87	1.51, 1.34	1.79	1.176 (1.155)	3	60	1691 (1917)	−226
revPBE	0.99	0.79, 0.64	1.85	1.180 (1.163)	4	58	1974 (1871)	−197
RPBE	1.01	0.77, 0.62	1.86	1.181 (1.164)	4	58	1671 (1865)	−193
TPSS	1.09	0.88, 0.74	1.86	1.177 (1.160)	3	59	1684 (1889)	−205
BP86	0.93	1.00, 0.86	1.83	1.180 (1.161)	4	59	1663 (1877)	−214
PBE0	1.60	0.33, 0.21	2.10	1.142 (1.142)	3	56	1967 (2032)	−65
TPSSh	1.40	0.53, 0.39	1.95	1.160 (1.152)	4	57	1803 (1942)	−140
MOHLYP	0.96	0.66, 0.47	1.86	1.186 (1.169)	4	58	1660 (1845)	−185
B97-2	1.54	0.24, 0.13	2.08	1.144 (1.143)	3	57	1939 (2017)	−78
B97-3	1.64	0.17, 0.07	2.23	1.142 (1.143)	2	57	1976 (1992)	−16
TPSSKCIS	1.01	0.90, 0.76	1.85	1.177 (1.160)	4	59	1678 (1884)	−206
MPWLYP1M	1.15	0.70, 0.55	1.89	1.174 (1.160)	3	58	1689 (1874)	−185
B1B95	1.59	0.32, 0.19	2.10	1.140 (1.140)	3	57	1969 (2034)	−65
Experimental	⋯	0.64[b]	1.88 ± .02 [c]	(1.151)[d]	+3/−8 [e]	59 ± 24 [e]	1801[f] (1876)[g]	−75

[a]First value calculated without CpC; value after comma calculated with CpC.
[b]Calculated from the experimental (Ref. 14) D_0 value of 0.57 ± 0.04 eV value together with the soft modes of frequencies 7, 34, 149, 169, and 225 cm^{-1} obtained with the M06 functional for the NO–$NiMg_8O_9$ cluster, and taking into account the decrease $\Delta\omega_e$ in the NO mode.
[c]References 22 and 27.
[d]Reference 31.
[e]Reference 22.
[f]Reference 26.
[g]Reference 30.

for the smaller cluster model. Similarly, Tables IV and VII show results for CO species interacting with the larger and with the smaller cluster models, respectively. For both adsorbates, these tables allow one to compare the results calculated with three meta-GGA exchange-correlation functionals from Minnesota (M0*x* functionals) with those obtained with the widely employed B3LYP hybrid GGA, and with the four other PBE0, B97-2, B97-3, and MPWLYP1M hybrid GGAs; with the BP86, PBE, PBEsol, SOGGA, revPBE, and RPBE GGAs; with the TPSS and TPSSKCIS meta GGAs; and with the TPSSh and B1B95 hybrid metafunctionals, as well as with the results in Tables I and II.

TABLE IV. Calculated results for gas-phase CO (values in parentheses) and for C-down adsorbed CO at a Ni^{2+} site on the Ni-doped MgO(100) surface. ($NiMg_{24}O_{25}$ model for D_e, R; $NiMg_8O_9$ model for ω_e and $\Delta\omega_e$. Values in parentheses are for separated CO. The θ(Ni–C–O) angle, Fig. 2, is in all cases close to zero degrees and is therefore not reported.)

Method	D_e (eV)	R(Ni–C) (Å)	R(C–O) (Å)	ω_e (cm^{-1})	$\Delta\omega_e$ (cm^{-1})
B3LYP	0.18, 0.06[a]	2.12	1.130 (1.127)	2174 (2219)	−45
M06-L	0.55, 0.42	1.98	1.138 (1.130)	2131 (2208)	−77
M06	0.42, 0.30	2.09	1.132 (1.125)	2210 (2246)	−37
M05	0.20, 0.10	2.14	1.132 (1.129)	2195 (2220)	−26
SOGGA	1.00, 0.82	1.83	1.152 (1.136)	2029 (2152)	−123
PBE	0.63, 0.47	1.89	1.151 (1.138)	2018 (2134)	−116
PBEsol	0.95, 0.77	1.84	1.151 (1.137)	2027 (2150)	−123
revPBE	0.37, 0.23	1.92	1.154 (1.142)	2009 (2116)	−107
RPBE	0.36, 0.21	1.92	1.154 (1.143)	2006 (2111)	−105
TPSS	0.54, 0.41	1.93	1.148 (1.137)	2038 (2143)	−105
BP86	0.53, 0.38	1.89	1.152 (1.139)	2013 (2127)	−114
PBE0	0.31, 0.19	2.09	1.128 (1.125)	2209 (2248)	−39
TPSSh	0.41, 0.28	2.01	1.138 (1.131)	2117 (2184)	−67
MOHLYP	0.14, −0.01	1.91	1.161 (1.148)	1976 (2086)	−110
B97-2	0.17, 0.09	2.11	1.129 (1.126)	2189 (2231)	−42
B97-3	0.12, 0.03	2.23	1.126 (1.125)	2225 (2220)	−5
TPSSKCIS	0.50, 0.36	1.93	1.148 (1.137)	2030 (2136)	−106
MPWLYP1M	0.35, 0.20	1.97	1.144 (1.135)	2053 (2143)	−90
B1B95	0.39, 0.16	2.12	1.126 (1.123)	2219 (2255)	−36
Experimental	0.37[b]	2.07 ± 0.02 [c,d]	1.15 ± 0.09 [c,d] (1.128)[f]	2152[e] (2143)[g]	+9

[a]First value calculated without CpCs; second value calculated with CpC.
[b]Calculated from the experimental (Ref. 14) D_0 value of 0.30 ± 0.03 eV value together with the soft modes of frequencies 128, 170, 216, 318, and 318 cm^{-1} obtained with the M06 functional for the NO–$NiMg_8O_9$ cluster, and taking into account the decrease $\Delta\omega_e$ in the CO mode.
[c]Reference 27.
[d]Reference 28.
[e]Reference 31.
[f]Reference 26.
[g]Reference 30.

First, the reported results show that the computed parameters are well converged with respect to the size of the model used to describe the Ni-doped Mg(100) surface. In fact, the maximum difference between the interaction energies calculated with the same exchange-correlation functional is 0.05 eV for NO and 0.02 eV for CO, both for the uncorrected or counterpoise-corrected bonding energies. Small variations are also found for other quantities, for example, a maximum of only 0.5 deg for O-Ni-N and Ni-N-O angles and a maximum difference of 0.003 Å for N-O bond lengths. In the case of the Ni-N distance, the largest difference found is 0.009 Å (for B3LYP). The results in the Appendix (Tables VI and

VII) may be consulted for further such comparisons, and we will discuss only those in Tables III and IV in the following discussion.

A. NO adsorbate

The second column of Table III shows the expectation value of S^2 for the Kohn–Sham determinant, where S is the total electron spin. The table shows substantial spin contamination of the Kohn–Sham determinant, for which $\langle S^2 \rangle$ varies between 0.87 (SOGGA and PBEsol) and 1.55 (B3LYP), significantly higher than the correct value of 0.75 for a doublet state. This is not necessarily an error since the Kohn–Sham determinant is not physical and, in principle, need not be a spin eigenfunction, but it is a measure of the complex open-shell character of the electronic states involved.

The experimental studies all report adsorption of the diatomics on NiO, whereas in the present work calculations are for adsorption on the Ni-doped MgO surface. Previous works compared results obtained with cluster models of the NiO and of the Ni-doped MgO surfaces.[15,18] For interaction of NO with the surfaces, it was found[15] that for a given method (i.e., a combination of density functional, basis set, and spin treatment, either polarized or unpolarized), the computed properties were the same within 0.12 eV for binding energies, 0.04 Å for the Ni–NO distance, and 2° for the tilt angle. An analogous comparison for adsorption of CO (Ref. 18 and entries 10–15 on Table II) shows that results for the two surfaces differ by at most 0.07 eV for binding energies and 0.03 Å for the Ni–CO distance. A similar effect on the binding energies (0.035 eV/Ni atom for NO to 0.025 eV/Ni atom for CO) was found in RMP2 calculations where calculations were performed for clusters with different numbers of Ni atoms (1–3 for NO and 1–5 for CO),[39] as noted above in Sec. II. Therefore, the differences between the models of the NiO(100) surface and of the Ni-doped MgO(100) surface are large enough that only a semiquantitative comparison can be established between the performance of the Ni-doped MgO theoretical model presented here and the NiO experimental results.

The comparison of the present B3LYP results with those reported previously by Pacchioni *et al.*,[18] which are included in the fifth row of Table I, shows small but noticeable differences caused by the use of different basis sets, a fixed adsorption tilt angle, and no relaxation of the cluster structure in the work of Pacchioni *et al.*[18] This is in agreement with the tiny but important energetic and geometric variations observed recently in the case of the CO/MgO(100) system.[19] The present energies are ~0.1 eV smaller than those reported by Pacchioni *et al.*,[18] i.e., farther from the experimental interaction energy, but the calculated vibrational frequency shift is now much closer (−87 cm^{-1}, this work, versus −110 cm^{-1}, Ref. 18). This is probably due to the 0.06 Å longer Ni–N distance calculated in this work.

Considering the interaction energies with CpC included, it is found that the functionals showing the smallest deviations with experiment are, in that order, revPBE and RPBE, which provide almost exact interaction energies, followed by MPWLYP1M, TPSS, TPSSKCIS, M06-L, MOHLYP, and M06. However, the CpC is known to often overestimate the BSSE, and sometimes the counterpoise-corrected interaction energy is farther from the complete basis set limit than is the uncorrected value. A prudent approach is often to include only half the CpC, i.e., to use the average of the corrected and uncorrected results. If we use that approach, the most accurate functionals for D_e are, in order, MPWLYP1M, followed by RPBE, revPBE, MOHLYP, M06, TPSS, TPSSh, TPSSKCIS, and M06-L. One sees in Table I that the CpCs for CASPT2 are much larger than those for DFT, but if we again take half the counterpoise and if we average the four CASPT2 results in Table I, CASPT2 would fit in the above list between TPSS and M06. Thus it is no longer true, as was sometimes claimed[14,15,18,39] in the past (where only older functionals were considered) that DFT is uncompetitive with WFT for this binding energy. This is especially important because DFT is more practical than correlated WFT for complex systems.

In the case of the local functional, M06-L, the binding is overestimated, a behavior similar to that presented by the ROBLYP approach (sixth row in Table I),[15,18] although the overestimate by M06-L is only about half as large. The overbinding by BLYP is associated with a too short adsorbate-to-surface distance, which results in a strong overlap of the NO π^* occupied orbital with the Ni 3d orbitals and in an excessive back donation of charge into the antibonding levels of NO, as already described by Pacchioni *et al.*[18] In contrast, the M06-L predicted value for the Ni–N distance is very accurate. The N–Ni distance calculated with most functionals, although generally close to experiment, is correlated with an exceedingly large N–O distance and a vibrational frequency shift differing by more than 100 cm^{-1} from the B3LYP and experimental values. This is true, in particular, for the functionals that give the best estimates of the interaction energy but it is not true for M06. For the latter, the Ni–N distance is much longer than the experimental one, but the frequencies are much smaller in absolute value and quite close to experiment. Importantly, the functionals that get vibrational frequency shifts closer to experiment have a Ni–N distance much longer than the experimental 1.88 Å. The best frequency shifts are those given by B97-2 followed by PBE0, B1B95, B3LYP, and MO5.

Of two functionals that have been shown to give accurate jellium surface energies, PBEsol and TPSS, the first strongly overestimates the NO–NiMgO interaction energy, whereas TPSS gives a rather good interaction energy. On the other hand, the RPBE functional, the second best functional for the NO–NiMgO interaction energy, does not reproduce the jellium surface energy.[82] The mean absolute value of the relative error in the jellium surface exchange correlation energy is known[82] for three of the functionals in the tables, in particular, BLYP, 35%; PBE, 4.9%; and RPBE, 8.5%. There is no straightforward correlation of these values for the artificial jellium system with the errors for the real adsorption systems studied in this article.

The addition of some HF exchange to the M06-L local functional plus reoptimization of the functional form produces the M06 functional, which significantly improves the agreement between the calculated and experimental vibra-

TABLE V. Direct comparison of PW91+U method to five density functional methods without a +U correction. (See Tables I–IV and text for details not repeated here.)

		NO				CO		
Method	X [a]	D_e (eV)	R(Ni–N) (Å)	θ(Ni–N–O) (deg)	$\Delta\omega$ (cm^{-1})	D_e (eV)	R(Ni–C) (Å)	$\Delta\omega$ (cm^{-1})
PW91+U	0	0.40	1.98	55	NA[b]	0.33	2.03	NA[b]
M06-L	0	0.86	1.89	59	−198	0.48	1.98	−77
revPBE	0	0.72	1.85	58	−197	0.30	1.92	−107
MPWLYP1M	5	0.62	1.89	58	−185	0.28	1.97	−90
TPSSh	10	0.46	1.95	57	−140	0.34	2.01	−67
M06	27	0.52	2.03	58	−101	0.36	2.09	−37
Experiment		0.64	1.88	59	−71	0.37	2.07	+9

[a]X is the percentage of HF exchange.
[b]NA denotes not available.

tional frequency shift (from -198 cm^{-1} with M06-L to -101 cm^{-1} with the M06 approach) although at the expense of a relatively more contaminated Kohn–Sham determinant (for the M06 functional, $\langle S^2 \rangle$ becomes 1.49). The M06 Ni–N bond length is elongated by 0.14 Å with respect to the M06-L value while the N–O bond is shortened by 0.02 Å. The optimized angles differ by less than 1°. It should be pointed out here that similar trends are observed in the calculated N–O distances of gaseous or adsorbed NO, i.e., the M06-L functional yields a larger N–O bond length than the M06 functional does for the free molecule and also for the supported NO species. Thus, for adsorption of NO on the Ni-doped MgO(100) surface, the M06 functional seems to be the best compromise since it gives reasonable binding energies and particularly because it provides a satisfactory NO vibrational frequency shift.

B. CO adsorption

Let us now turn our attention to what happens when the same functionals are employed to study the interaction of CO with the Ni-doped MgO(100) surface, with results given in Table IV. We see that the computational approaches considered in the present work predict negative vibrational frequency shifts (ranging between -5 and -123 cm^{-1}) while the experimental frequency shift is positive (+9 cm^{-1}). The counterpoise-corrected interaction energy calculated with the B3LYP approach (0.06 eV or, if only half the correction is used, 0.12 eV) is rather small when compared with the experimental result (0.37 eV) but the geometrical parameters are in excellent agreement with the experimental ones.[27,28,31] The calculated B3LYP vibrational frequency shift is -45 cm^{-1}. The M06-L functional still predicts a 0.1 Å too short Ni–C distance, but, as for NO interacting with the Ni-doped MgO(100) surface, it agrees better with experiment than all of the local GGA functionals and the TPSS, meta-GGA, which give significantly too short distances, whereas at one time[27,28] DFT was thought to overestimate this distance. The best Ni–C distances are predicted by PBE0, M06, B97-2, B3LYP, B1B95, and M05. With respect to the performance of the Minnesota functionals for the binding energy, it appears that the M06-L functional slightly overestimates the binding energy between CO and the oxide substrate (>0.4 eV), that the M06 functional yields very good interaction energies (0.36 eV if one uses half the CpC), and that the M05 functional gives the vibrational frequency shift (-26 cm^{-1}) closest to experiment, in agreement with the findings discussed above for NO interacting with the same substrate. With full CpC, the best interaction energies are those given by BP86, TPSSKCIS, TPSS, M06-L, and M06. Nevertheless, the M06-L binding energy is only ~0.1 eV larger than the experimental value. The M05 energies are similar to those calculated with the B3LYP approach and, hence, they are too low. Again, PBEsol and SOGGA give a strong overbinding when compared with experiment. If one uses half the CpC, the nine best functionals for D_e, in ranked order, are M06, TPSSh, TPSSKCIS, revPBE, BP86, RPBE, MPWLYP1M, TPSS, and M06-L, which are the same functionals as appearing on the corresponding list for NO, except that MOHLYP appears only in the first list and BP86 appears only in the second list. MOHLYP would be number 17 in the second list and BP86 would be number 10 in the first list. Averaging these functionals in order of their average rank on the two lists gives M06, revPBE, RPBE, TPSSh, and MPWLYP1M, TPSSKCIS, TPSS, BP86, and M06-L. CASPT2 has an error for CO that is twice as large as M06-L and so is not competitive in this ranking. This shows the great progress that DFT has made!

None of the functionals give the correct sign for the frequency shift. The physical effects involved in the CO frequency shift are discussed in a previous paper,[91] which also showed that this provides a difficult test.

As mentioned in the introduction, some workers obtained the best agreement with experiment for NO with a PW91+U calculation where +U denotes adding an empirical on-site Coulomb interaction term;[40] they also obtained their best agreement with experiment for CO with the PW91+U treatment[42] (for CO, the LSDA+U method could not provide a good fit to all properties examined with the same physically reasonable U). How does this method compare with the results obtained here with better functionals without resorting to a U parameter? To answer this question, Table V presents a direct comparison of the PW91+U results to the results for four of the five best performing density functionals for D_e (RPBE is not included in Table V because its results are always very similar to the similar but older revPBE func-

TABLE VI. Calculated results for gas-phase NO (values in parentheses) and for N-down adsorbed NO on top of a Ni^{2+} site on the $NiMg_8O_9$ model of the Ni-doped MgO(100) surface.

Method	$\langle \hat{S}^2 \rangle$	D_e without CpC (eV)	D_e with CpC (eV)	R(Ni–N) (Å)	R(N–O) (Å)	θ(O–Ni–N) (deg)	θ(Ni–N–O) (deg)
B3LYP	1.54	0.25	0.16	2.08	1.150 (1.147)	4	57
M06-L	1.18	0.91	0.80	1.89	1.167 (1.150)	3	59
M06	1.49	0.56	0.46	2.02	1.145 (1.141)	3	58
M05	1.48	0.36	0.26	2.03	1.145 (1.144)	4	57
SOGGA	0.87	1.54	1.40	1.79	1.178 (1.155)	3	60
PBE	1.22	1.08	0.96	1.83	1.180 (1.160)	4	59
PBEsol	0.87	1.50	1.36	1.79	1.178 (1.156)	3	60
revPBE	1.00	0.76	0.64	1.86	1.181 (1.163)	4	58
RPBE	1.01	0.74	0.62	1.87	1.182 (1.164)	4	58
TPSS	1.33	0.87	0.76	1.86	1.179 (1.160)	4	59
BP86	0.93	0.99	0.87	1.83	1.182 (1.161)	4	59
PBE0	1.59	0.30	0.21	2.09	1.143 (1.142)	3	56
TPSSh	1.40	0.50	0.39	1.95	1.162 (1.152)	5	57
MOHLYP	0.96	0.61	0.48	1.86	1.186 (1.169)	5	57
B97-2	1.54	0.22	0.14	2.08	1.144 (1.143)	3	56
B97-3	1.64	0.15	0.08	2.22	1.143 (1.143)	3	57
TPSSKCIS	1.02	0.89	0.77	1.85	1.179 (1.160)	4	59
MPWLYP1M	1.15	0.67	0.56	1.90	1.176 (1.160)	4	58
B1B95	1.59	0.29	0.19	2.10	1.141 (1.140)	4	57

tional) and for M06-L because its good predictions for one of the geometries. The PW91+U functional is not better than these functionals that do not have a +U parameter.

IV. CONCLUSIONS

The adsorption of NO or CO on the Ni-doped MgO(100) surface has been studied using the B1B95, M05, M06, and TPSSh hybrid metafunctionals, the M06-L, TPSS, and TPSSKCIS meta-GGA functionals, the B3LYP, MPWLYP1M, PBE0, B97-2, and B97-3 hybrid GGAs, and the BP86, PBE, PBEsol, revPBE, RPBE, MOHLYP, and SOGGA GGAs. The three Minnesota functionals included in the present study are those with percentages of HF exchange below 30, which are the only ones recommended for applications to systems containing transition metals.

The comparison to experiment has uncertainties due to BSSE and the assumption that the Ni-doped MgO theoretical model developed here can be compared with the reported NiO experimental results. Nevertheless, our best attempt to judge the methods despite these difficulties yields the following conclusions. We found that none of the density functionals explored is able to simultaneously provide accurate Ni-X and X-O (X=C or N) distances, interaction energies, and vibrational frequency shifts for either CO or NO adsorption on the surface. In the case of NO, MPWLYP1M, revPBE, RPBE, and M06 provide the best estimates of the interaction energy, while the best vibrational frequency shifts are predicted by the B97-2, PBE0, B1B95, and B3LYP methods. In the case of CO, the best estimates of the interaction energy are obtained with the M06, TPSSh, TPSSKCIS, and revPBE, and the best vibrational frequency shifts are predicted by the B97-3, M05, B1B95, and M06 functionals (which, however, all give the wrong sign). Overall, the binding energy is best described with (in order) M06, revPBE, RPBE, TPSSh,

TABLE VII. Calculated results for gas-phase CO (values in parentheses) and for C-down adsorbed CO on top of a Ni^{2+} site on the $NiMg_8O_9$ model of the Ni-doped MgO(100) surface. [The θ(Ni–C–O) angle is in all cases close to zero degrees.]

Method	D_e without CpC (eV)	D_e with CpC (eV)	R(Ni–C) (Å)	R(C–O) (Å)
B3LYP	0.16	0.06	2.10	1.131 (1.127)
M06-L	0.55	0.44	1.96	1.139 (1.130)
M06	0.40	0.29	2.07	1.128 (1.125)
M05	0.20	0.09	2.11	1.132 (1.129)
SOGGA	0.99	0.82	1.83	1.153 (1.137)
PBE	0.62	0.48	1.88	1.152 (1.138)
PBEsol	0.93	0.77	1.84	1.153 (1.136)
revPBE	0.37	0.24	1.91	1.154 (1.142)
RPBE	0.35	0.23	1.92	1.155 (1.144)
TPSS	0.54	0.41	1.92	1.149 (1.137)
BP86	0.53	0.39	1.89	1.153 (1.139)
PBE0	0.29	0.18	2.07	1.128 (1.125)
TPSSh	0.39	0.27	1.99	1.139 (1.131)
MOHLYP	0.13	0.00	1.92	1.161 (1.148)
B97-2	0.17	0.07	2.09	1.129 (1.126)
B97-3	0.11	0.02	2.20	1.127 (1.125)
TPSSKCIS	0.50	0.37	1.92	1.149 (1.137)
MPWLYP1M	0.33	0.20	1.96	1.145 (1.135)
B1B95	0.26	0.14	2.10	1.126 (1.123)

MPWLYP1M, TPSSKCIS, TPSS, BP86, and M06-L, but several of these functionals strongly overestimate the magnitude of both the NO and CO vibrational frequency shifts on adsorption. An important general conclusion is that a functional that produces a good jellium surface energy might give large errors for molecule-surface interaction energies.

The comparison of the results obtained with each of the exchange-correlation potentials considered here on the NO and CO interaction with the Ni-doped MgO(100) surface allows us to conclude that the M06 functional is the best choice overall for the simultaneous description of geometries, interaction energies, and X-O (X=C or N) vibrational frequency shifts. But further improvement is needed for calculating vibrational frequency shifts with any of the functionals.

ACKNOWLEDGMENTS

The authors are grateful to Yan Zhao and Nate Schulz for helpful assistance. Financial support was provided by the Spanish Ministerio de Ciencia en Innovación (MICINN Grant No. FIS2008-02238), Generalitat de Catalunya (Grant Nos. 2009SGR1041 and XRQTC), and by the COST-D41 action. This work was supported in part by the U.S. Air Force Office of Scientific Research under Grant No. FA9550-08-1-0183.

APPENDIX: RESULTS FOR CO AND NO ADSORPTION FOR $NiMg_8O_9$ MODEL CLUSTER

The appendix presents tables of results with the smaller clusters. These results, Tables VI and VII, are presented mainly to show that the values discussed in Sec. III are well converged with respect to cluster size.

[1] G. A. Somorjai and Y. Borodko, Catal. Lett. **59**, 89 (1999).
[2] H.-J. Freund, Faraday Trans. **114**, 1 (1999).
[3] B. Hammer, L. B. Hansen, and J. K. Nørskov, Phys. Rev. B **59**, 7413 (1999).
[4] P. Strasser, Q. Fan, M. Devenney, W. H. Weinberg, P. Liu, and J. K. Nørskov, J. Phys. Chem. B **107**, 11013 (2003).
[5] K. Honkala, A. Hellman, I. N. Remediakis, A. Logadottir, A. Carlsson, S. Dahl, C. H. Christensen, and J. K. Nørskov, Science **307**, 555 (2005).
[6] C. H. Christensen and J. K. Nørskov, J. Chem. Phys. **128**, 182503 (2008).
[7] S. Furuyama, H. Fujii, M. Kawamura, and T. Morimoto, J. Phys. Chem. **82**, 1028 (1978).
[8] E. A. Paukshtis, R. I. Soltanov, and N. E. Yurchenko, React. Kinet. Catal. Lett. **16**, 93 (1981).
[9] C. R. Henry, C. Chapon, and C. Duriez, J. Chem. Phys. **95**, 700 (1991).
[10] J. W. He, C. A. Estrada, J. S. Corneille, M. C. Wu, and D. W. Goodman, Surf. Sci. **261**, 164 (1992).
[11] D. Scarano, G. Spoto, S. Bordiga, S. Coluccia, and A. Zecchina, J. Chem. Soc., Faraday Trans. **88**, 291 (1992).
[12] L. Chen, R. Wu, N. Kioussis, and Q. Zhang, Chem. Phys. Lett. **290**, 255 (1998).
[13] F. Illas, G. Pacchioni, A. Pelmenschikov, L. G. M. Petterson, R. Dovesi, C. Pisani, K. M. Neyman, and N. Rösch, Chem. Phys. Lett. **306**, 202 (1999).
[14] R. Wichtendahl, M. Rodríguez-Rodrigo, U. Härtel, H. Kuhlenbeck, and H.-J. Freund, Surf. Sci. **423**, 90 (1999).
[15] C. Di Valentin, G. Pacchioni, T. Bredow, D. Dominguez-Ariza, and F. Illas, J. Chem. Phys. **117**, 2299 (2002).
[16] Y. Xu, J. Li, Y. Zhang, and W. Chen, Surf. Sci. **525**, 13 (2003).
[17] G. Spoto, E. N. Gribov, G. Ricchiardi, A. Damin, D. Scarano, S. Bordiga, C. Lamberti, and A. Zecchina, Prog. Surf. Sci. **76**, 71 (2004).
[18] G. Pacchioni, C. Di Valentin, D. Dominguez-Ariza, F. Illas, T. Bredow, T. Klüner, and V. Staemmler, J. Phys.: Condens. Matter **16**, S2497 (2004).
[19] R. Valero, J. R. B. Gomes, D. G. Truhlar, and F. Illas, J. Chem. Phys. **129**, 124710 (2008).
[20] C. Xu, W. S. Oh, and D. W. Goodman, J. Phys. Chem. B **104**, 10310 (2000).
[21] J. A. Rodriguez, T. Jirsak, M. Pérez, L. González, and A. Maiti, J. Chem. Phys. **114**, 4186 (2001).
[22] R. Lindsay, P. Baumgärtel, R. Terborg, O. Schaff, A. M. Bradshaw, and D. P. Woodruff, Surf. Sci. **425**, L401 (1999).
[23] E. Escalona Platero, S. Coluccia, and A. Zecchina, Langmuir **1**, 407 (1985).
[24] E. Escalona Platero, S. Coluccia, and A. Zecchina, Surf. Sci. **171**, 465 (1986).
[25] E. Escalona Platero, B. Fubini, and A. Zecchina, Surf. Sci. **179**, 404 (1987).
[26] E. Escalona Platero, D. Scarano, A. Zecchina, G. Meneghini, and R. De Franceschi, Surf. Sci. **350**, 113 (1996).
[27] J.-T. Hoeft, M. Kittel, M. Polcik, S. Bao, R. L. Toomes, J.-H. Kang, D. P. Woodruff, M. Pascal, and C. L. A. Lamont, Phys. Rev. Lett. **87**, 086101 (2001).

[28] M. Kittel, J.-T. Hoeft, S. Bao, M. Polcik, R. L. Toomes, J.-H. Kang, D. P. Woodruff, M. Pascal, and C. L. A. Lamont, Surf. Sci. **499**, 1 (2002).
[29] H. Kuhlenbeck, G. Odörfer, R. Jaeger, G. Illing, M. Menges, Th. Mull, H.-J. Freund, M. Pöhlchen, V. Staemmler, S. Witzel, C. Scharfschwerdt, K. Wennemann, T. Liedtke, and M. Nuemann, Phys. Rev. B **43**, 1969 (1991).
[30] K. P. Huber and G. Herzberg, *Molecular Spectra and Molecular Structure* (Van Nostrand Reinhold, New York, 1979).
[31] K. P. Huber and G. Herzberg, NIST Chemistry WebBook, NIST Standard Reference Database No. 69, edited by P. J. Linstrom and W. G. Mallard (National Institute of Standards and Technology, Gaithersburg, MD, 2008).
[32] L. H. Coudert, V. Dana, J.-Y. Mandin, M. Morillon-Chapey, R. Farrenq, and G. Guelachvili, J. Mol. Spectrosc. **172**, 435 (1995).
[33] Y. Zhao and D. G. Truhlar, Acc. Chem. Res. **41**, 157 (2008).
[34] E. Giamello, E. Garrone, E. Guglielminotti, and A. Zecchina, J. Mol. Catal. **24**, 59 (1984).
[35] M. Pöhlchen and V. Staemmler, J. Chem. Phys. **97**, 2583 (1992).
[36] T. Klüner, H.-J. Freund, J. Freitag, and V. Staemmler, J. Chem. Phys. **104**, 10030 (1996).
[37] T. Klüner, H.-J. Freund, J. Freitag, and V. Staemmler, J. Mol. Catal. Chem. **119**, 155 (1997).
[38] T. Klüner, S. Thiel, H.-J. Freund, and V. Staemmler, Chem. Phys. Lett. **294**, 413 (1998).
[39] I. Mehdaoui and T. Klüner, J. Phys. Chem. A **111**, 13233 (2007).
[40] A. Rohrbach and J. Hafner, Phys. Rev. B **71**, 045405 (2005).
[41] T. Bredow, J. Phys. Chem. B **106**, 7053 (2002).
[42] A. Rohrbach, J. Hafner, and G. Kresse, Phys. Rev. B **69**, 075413 (2004).
[43] A. D. Becke, Phys. Rev. A **38**, 3098 (1988).
[44] C. Lee, W. Yang, and R. G. Parr, Phys. Rev. B **37**, 785 (1988).
[45] A. D. Becke, J. Chem. Phys. **98**, 5648 (1993).
[46] P. J. Stephens, F. J. Devlin, C. F. Chabalowski, and M. J. Frisch, J. Phys. Chem. **98**, 11623 (1994).
[47] C. Adamo and V. Barone, J. Chem. Phys. **108**, 664 (1998).
[48] R. Valero, R. Costa, I. P. R. Moreira, D. G. Truhlar, and F. Illas, J. Chem. Phys. **128**, 114103 (2008).
[49] I. V. Yudanov, V. A. Nasluzov, K. M. Neyman, and N. Rösch, Int. J. Quantum Chem. **65**, 975 (1997).
[50] N. López and F. Illas, J. Phys. Chem. **102**, 1430 (1998).
[51] G. Pacchioni and A. M. Ferrari, Catal. Today **50**, 533 (1999).
[52] R. Soave and G. Pacchioni, Chem. Phys. Lett. **320**, 345 (2000).
[53] J. R. B. Gomes, F. Illas, N. Cruz Hernández, J. F. Sanz, A. Wander, and N. M. Harrison, J. Chem. Phys. **116**, 1684 (2002).
[54] J. R. B. Gomes, F. Illas, N. Cruz Hernández, A. Márquez, and J. F. Sanz, Phys. Rev. B **65**, 125414 (2002).
[55] J. R. B. Gomes, Z. Lodziana, and F. Illas, J. Phys. Chem. B **107**, 6411 (2003).
[56] F. Cinquini, C. Di Valentim, E. Finazzi, L. Giordano, and G. Pacchioni, Theor. Chem. Acc. **117**, 827 (2007).
[57] L. E. Roy, P. J. Hay, and R. L. Martin, J. Chem. Theory Comput. **4**, 1029 (2008).
[58] P. J. Hay and W. R. Wadt, J. Chem. Phys. **82**, 299 (1985).
[59] A. Schäfer, C. Huber, and R. Ahlrichs, J. Chem. Phys. **100**, 5829 (1994).
[60] Y. Zhao and D. G. Truhlar, J. Chem. Phys. **125**, 194101 (2006).
[61] Y. Zhao and D. G. Truhlar, Theor. Chem. Acc. **120**, 215 (2008).
[62] Y. Zhao, N. E. Schultz, and D. G. Truhlar, J. Chem. Phys. **123**, 161103 (2005).
[63] J. P. Perdew, Phys. Rev. B **33**, 8822 (1986).
[64] J. P. Perdew, K. Burke, and M. Enrzerhof, Phys. Rev. Lett. **77**, 3865 (1996); **78**, 1396(E) (1997).
[65] J. P. Perdew, A. Ruzsinszky, G. I. Csonka, O. A. Vydrov, G. E. Scuseria, L. A. Constantin, X. Zhou, and K. Burke, Phys. Rev. Lett. **100**, 136406 (2008).
[66] Y. Zhao and D. G. Truhlar, J. Chem. Phys. **128**, 184109 (2008).
[67] Y. Zhang and W. Yang, Phys. Rev. Lett. **80**, 890 (1998).
[68] N. E. Schultz, Y. Zhao, and D. G. Truhlar, J. Phys. Chem. A **109**, 11127 (2005).
[69] C. Adamo, M. Cossi, and V. Barone, J. Mol. Struct.: THEOCHEM **493**, 145 (1999).
[70] M. Ernzerhof and G. E. Scuseria, J. Chem. Phys. **110**, 5029 (1999).
[71] P. J. Wilson, T. J. Bradley, and D. J. Tozer, J. Chem. Phys. **115**, 9233 (2001).
[72] T. W. Keal and D. J. Tozer, J. Chem. Phys. **123**, 121103 (2005).
[73] J. Tao, J. P. Perdew, V. N. Staroverov, and G. E. Scuseria, Phys. Rev. Lett. **91**, 146401 (2003).
[74] V. N. Staroverov, G. E. Scuseria, J. Tao, and J. P. Perdew, J. Chem. Phys. **119**, 12129 (2003).
[75] J. Rey and A. Savin, Int. J. Quantum Chem. **69**, 581 (1998).
[76] J. B. Krieger, J. Chen, G. J. Iafrate, and A. Savin, in *Electron Correlations and Materials Properties*, edited by A. Gonis and N. Kioussis (Plenum, New York, 1999), p. 463.
[77] J. Toulouse, A. Savin, and C. Adamo, J. Chem. Phys. **117**, 10465 (2002).
[78] A. D. Becke, J. Chem. Phys. **104**, 1040 (1996).
[79] J. P. Perdew and Y. Wang, Phys. Rev. B **45**, 13244 (1992).
[80] J. P. Perdew, J. A. Chevary, S. H. Vosko, K. A. Jackson, M. R. Pederson, D. J. Singh, and C. Fiolhais, Phys. Rev. B **46**, 6671 (1992).
[81] J. P. Perdew, J. A. Chevary, S. H. Vosko, K. A. Jackson, M. R. Pederson, D. J. Singh, and C. Fiolhais, Phys. Rev. B **48**, 4978(E) (1993) .
[82] S. Kurth, J. P. Perdew, and P. Blaha, Int. J. Quantum Chem. **75**, 889 (1999).
[83] F. Viñes, C. Sousa, F. Illas, P. Liu, and J. A. Rodriguez, J. Phys. Chem. C **111**, 1307 (2007).
[84] S. F. Sousa, P. A. Fernandes, and M. J. Ramos, J. Phys. Chem. A **111**, 10439 (2007).
[85] A. D. Becke, J. Chem. Phys. **107**, 8554 (1997).
[86] V. N. Staroverov, G. E. Scuseria, J. Tao, and J. P. Perdew, Phys. Rev. B **69**, 075102 (2004).
[87] Y. Zhao, J. Pu, B. J. Lynch, and D. G. Truhlar, Phys. Chem. Chem. Phys. **6**, 673 (2004).
[88] S. F. Boys and F. Bernardi, Mol. Phys. **19**, 553 (1970).
[89] M. J. Frisch, G. W. Trucks, H. B. Schlegel, *et al.*, GAUSSIAN03, Revision D.01, Gaussian, Inc., Wallingford, CT, 2004.
[90] Y. Zhao and D. G. Truhlar, MN-GFM 4.3, University of Minnesota, Minneapolis, 2009.
[91] N. E. Schultz, B. F. Gherman, C. J. Cramer, and D. G. Truhlar, J. Phys. Chem. B **110**, 24030 (2006).